

Cronin effect and energy conservation constraints in high energy proton-nucleus collisions

Enrico Cattaruzza and Daniele Treleani

Dipartimento di Fisica Teorica dell'Università di Trieste
and INFN, Sezione di Trieste,
Strada Costiera 11, Miramare-Grignano, I-34014 Trieste, Italy.

Abstract

We estimate the Cronin effect in pA collisions at the CERN LHC and at RHIC, using a Glauber-Eikonal model of initial state multiparton interactions. For a correct determination of the initial parton flux, we upgrade the model cross section, taking carefully into account all kinematical constraints of each multi-parton interaction process. As compared with previous results, derived with approximate kinematics, we obtain a softer spectrum of produced partons, while improving the agreement of the model with the recent measurements of π^0 production in $d + Au$ collisions at $\sqrt{s} = 200$ AGeV.

E-mail ecattar@ts.infn.it
E-mail daniel@trieste.infn.it

1 Introduction

Hadron-nucleus interactions represent an intermediate regime between hadron-hadron and nucleus-nucleus collisions, where different ideas on the role played by the complexity of the target on large p_t dynamics may be tested [1]. Of particular interest is the study of the Cronin effect [2, 3], namely the deformation of the transverse spectrum of particles, or jets, produced in hadron-nucleus collisions in the projectile fragmentation region. Given the large scale of momentum transfer in the process, the problem is within reach of a perturbative approach, while the effects of the complex structure of the target may be controlled by changing energy and atomic mass number.

The effect is originated by the high density of the nuclear target, which induces the projectile's partons interacting simultaneously with several partons of the target. There is not however a unique explanation of the underlying dynamical mechanism [4, 5, 6, 7, 8] and different approaches can only be discriminated by measuring the large p_t spectra in hadron nucleus collisions at the energies of the future colliders, where various models give different predictions. In our opinion, the simplest approach is to adopt the Glauber prescription of factorization of the overall many-parton S matrix, as a product of elementary partonic S matrices [9]. Since production at the parton level represents a higher order correction in the coupling constant, the natural zeroth order approximation is obtained when evaluating each elementary parton interaction at the lowest order in α_S , which leads considering binary processes only.

Encouragingly a recent calculation, based on this simplest scheme [10], compares rather reasonably with the latest experimental measurements, due to the PHENIX collaboration, of the Cronin effect in large p_t pion production in $d+Au$ collisions, at a center of mass energy of 200 AGeV [11].

It's remarkable that in such an approach, when adopting the usual approximations of the Glauber picture of high energy hadron-nucleus collisions, the whole effect of the nuclear target medium may be taken into account exactly, in the evaluation of the inclusive transverse spectrum [9]. After summing all possible multi-parton interactions of the projectile one in fact obtains

$$\frac{d\sigma}{d^2b dx d^2p_t} = \frac{1}{(2\pi)^2} \int d^2r e^{ip_t r} G(x) S_{hard}^A(\bar{r}, \bar{b}, p_0) \quad (1)$$

where

$$S_{hard}^A(\bar{r}, \bar{b}, p_0) = \left[e^{T_A(b)[F_A(x, r) - F_A(x, 0)]} - e^{-T_A(b)F_A(x, 0)} \right]$$

and $T_A(b)$ is the usual nuclear thickness, as a function of the hadron-nucleus impact parameter b , $G(x)$ the parton number density of the projectile, as a function of the fractional momentum x , p_t the transverse momentum of the final observed parton and

$$F_A(x, b) = \int \frac{d^2 p_t}{(2\pi)^2} dx' G_A(x') \frac{d\hat{\sigma}}{d^2 p_t} e^{ip_t b} \quad (2)$$

In Eq.(2) $G_A(x')$ is the parton number density of the target nucleus, divided by the atomic mass number A , as a function of the fractional momentum x' , and $d\hat{\sigma}/d^2 p_t$ the elementary parton-parton scattering cross section, which includes also the kinematical limits constraints. For sake of simplicity flavor dependence is not written explicitly. The quantity $S_{hard}^A(\bar{r}, \bar{b}, p_0)$ can be interpreted in terms of dipole-nucleus hard cross section. The dipole originates from the square of the scattering amplitude, expressed as a function of the Fourier variable \bar{r} , corresponding to the transverse size of the dipole [12].

By expanding Eq.(1) as a power series in $\hat{\sigma}$, one obtains all different multiple scatterings of the projectile parton. As a consequence of the Glauber prescription of factorization of the overall many-parton S matrix, each term in the expansion is represented by an incoherent convolution of binary partonic collisions [9, 13]. Analogously to the case of the Glauber approach to hadron-nucleus processes, the S -matrix factorization prescription does not however imply any space-time ordering between the different elementary collisions. It only implies that a connected n -body interaction process is well approximated by a product of two-body interactions, which corresponds to the dominance of the pole contribution, in a dispersive representation of the projectile-exchanged gluon amplitude [14].

All expressions are divergent for small values of the lower cutoff in p_t , which sets the regime of hard interactions. Nevertheless, as unitarity is explicitly implemented, each term in the series expansion of Eq.(1) contains subtractions, which lower the degree of the infrared singularity, from an inverse power to a power of a logarithm of the cutoff [13]. It's also worth mentioning that, in this model, the average energy, carried by the partons scattered to the final state is bound to be smaller than the overall initial state energy [15], whereas such a quantity is divergent as an inverse power of the cutoff, if evaluated in impulse approximation.

The approach to hard processes in hadron-nucleus collisions, based on the factorization of the multi-parton S matrix, is hence unitary and satisfies various non-trivial consistency requirements, including the AGK cutting rules [16]. As $p_t \rightarrow 0$ the importance of unitarity corrections grows, producing a suppression of the integrated parton yield and a random walk of partons to higher p_t , recovering in this way the local isotropy in transverse space of the black disk limit, which is, on the contrary, maximally broken by the lowest order impulse approximation term [15].

The model hence contains geometrical shadowing at low p_t and Cronin enhancement of the transverse spectrum at moderate p_t . Some non secondary features of the interaction are not accounted however, as one expects genuine dynamical shadowing at low x , due to non-linear gluon interactions. On the other hand also the simplifying assumptions adopted in the derivation of Eq.(1) require a closer inspection. More specifically, to obtain Eq.(1), one needs to

decouple longitudinal and transverse degrees of freedom, while conserving the longitudinal momentum components in the interaction. Kinematical constraints are hence implemented only approximately, in such a way that final state partons turn out to be more energetic than the initial ones, the effect being emphasized when the number of re-scatterings grows. The final p_t spectrum gets hence shifted towards larger transverse momenta which, given the steepness of parton distributions at small x , might modify appreciably the evaluation of the Cronin effect.

The purpose of the present note is to investigate this specific aspect of the model more closely. We hence compare the spectrum, obtained by implementing exactly all kinematical constraints, with the summed expression in Eq.(1), both at the LHC regime and in the kinematical domain of the measurements of the Cronin effect in $d + Au \rightarrow \pi^0 X$, recently performed by the PHENIX Collaboration.

2 Transverse Spectrum

The expression in Eq.(1) represents the sum of all possible collisions of the observed parton with the different scattering centers of the target nucleus. When the kinematical constraints are implemented exactly, the multi-scattering series cannot be re-summed any more in a closed analytic expression and each different term needs to be evaluated separately. Most of the spectrum is nevertheless well reproduced by the the first three terms of the expansion [13]. Hence we approximate the cross section by:

$$\frac{d\sigma}{d^2p_t dy d^2b} = \sum_i \frac{d\sigma_i}{d^2p_t dy d^2b} \quad (3)$$

where p_t is the transverse momentum of the observed parton, y its rapidity, b the impact parameter of the collision and the sum runs over the different species of projectile partons, while

$$\frac{d\sigma_i}{d^2p_t dy d^2b} = \frac{d\sigma_i^{(1)}}{d^2p_t dy d^2b} + \frac{d\sigma_i^{(2)}}{d^2p_t dy d^2b} + \frac{d\sigma_i^{(3)}}{d^2p_t dy d^2b} \quad (4)$$

where

$$\begin{aligned} \frac{d\sigma_i^{(1)}}{d^2p_t dy d^2b} &= T_A(b) \sum_j \frac{1}{1 + \delta_{ij}} \int d^2q_1 dx' \delta^{(2)}(\bar{q}_1 - \bar{p}_t) \hat{\sigma_{ij}}^{(1)}(y, x'; q_1) \\ &\times x \left[f_{\frac{x}{p}}(x, Q_{fct}) f_{\frac{x'}{A}}(x', Q_{fct}) + f_{\frac{x'}{p}}(x', Q_{fct}) f_{\frac{x}{A}}(x, Q_{fct}) \right] \end{aligned}$$

is the single scattering term (the projectile parton interacts with a single parton of the target and vice-versa),

$$\begin{aligned}
\frac{d\sigma_i^{(2)}}{d^2 p_t dy d^2 b} &= \frac{1}{2!} T_A(b)^2 \sum_{j,k} \frac{1}{1 + \delta_{ij}} \frac{1}{1 + \delta_{ik}} \int d^2 q_1 d^2 q_2 dx' dx'' \\
&\times \left[\delta^{(2)}(\bar{q}_1 + \bar{q}_2 - \bar{p}_t) - \delta^{(2)}(\bar{q}_1 - \bar{p}_t) - \delta^{(2)}(\bar{q}_2 - \bar{p}_t) \right] \\
&\times x f_{\frac{i}{p}}(x, Q_{fct}) f_{\frac{j}{A}}(x', Q_{fct}) f_{\frac{k}{A}}(x'', Q_{fct}) \hat{\sigma}_{ijk}^{(2)}(y, x', x''; \bar{q}_1, \bar{q}_2)
\end{aligned}$$

is the rescattering term (the projectile parton interacts with two different partons of the target), and

$$\begin{aligned}
\frac{d\sigma_i^{(3)}}{d^2 p_t dy d^2 b} &= \frac{1}{3!} T_A(b)^3 \sum_{j,k,l} \frac{1}{1 + \delta_{ij}} \frac{1}{1 + \delta_{ik}} \frac{1}{1 + \delta_{il}} \int d^2 q_1 d^2 q_2 d^2 q_3 \\
&\times dx' dx'' dx''' \hat{\sigma}_{ijkl}^{(3)}(y, x', x'', x'''; \bar{q}_1, \bar{q}_2, \bar{q}_3) \\
&\times \left[\delta^{(2)}(\bar{q}_1 + \bar{q}_2 + \bar{q}_3 - \bar{p}_t) - \delta^{(2)}(\bar{q}_1 + \bar{q}_2 - \bar{p}_t) - \delta^{(2)}(\bar{q}_2 + \bar{q}_3 - \bar{p}_t) \right. \\
&\times \left. - \delta^{(2)}(\bar{q}_3 + \bar{q}_1 - \bar{p}_t) + \delta^{(2)}(\bar{q}_1 - \bar{p}_t) + \delta^{(2)}(\bar{q}_2 - \bar{p}_t) + \delta^{(2)}(\bar{q}_3 - \bar{p}_t) \right] \\
&\times x f_{\frac{i}{p}}(x, Q_{fct}) f_{\frac{j}{A}}(x', Q_{fct}) f_{\frac{k}{A}}(x'', Q_{fct}) f_{\frac{l}{A}}(x''', Q_{fct}).
\end{aligned}$$

is the double rescattering term (the projectile parton interacts with three different partons of the target).

The subtraction terms, in the rescattering and in the double rescattering terms, are a direct consequence of the implementation of unitarity in the process. The sums run over the different species of target partons. The quantities $f_{\frac{j}{A}}(x', Q_{fct})$ represent the nuclear parton distributions, while the multiparton interaction cross sections are given by:

$$\begin{aligned}
\hat{\sigma}_{ij}^{(1)}(y, x'; q_1) &= k_{factor} \frac{d\hat{\sigma}_{ij}(\hat{s}_1, \hat{t}_1, \hat{u}_1)}{d\hat{t}_1} \Theta(\Phi^{(1)}) \\
\hat{\sigma}_{ijk}^{(2)}(y, x', x''; \bar{q}_1, \bar{q}_2) &= (k_{factor})^2 \frac{d\hat{\sigma}_{ik}(\hat{s}_2, \hat{t}_2, \hat{u}_2)}{d\hat{t}_2} \frac{d\hat{\sigma}_{ij}(\hat{s}_1, \hat{t}_1, \hat{u}_1)}{d\hat{t}_1} \Theta(\Phi^{(2)}) \Theta(\Phi^{(1)}) \\
\hat{\sigma}_{ijkl}^{(3)}(y, x', x'', x'''; \bar{q}_1, \bar{q}_2, \bar{q}_3) &= (k_{factor})^3 \frac{d\hat{\sigma}_{il}(\hat{s}_3, \hat{t}_3, \hat{u}_3)}{d\hat{t}_3} \frac{d\hat{\sigma}_{ik}(\hat{s}_2, \hat{t}_2, \hat{u}_2)}{d\hat{t}_2} \\
&\times \frac{d\hat{\sigma}_{ij}(\hat{s}_1, \hat{t}_1, \hat{u}_1)}{d\hat{t}_1} \Theta(\Phi^{(3)}) \Theta(\Phi^{(2)}) \Theta(\Phi^{(1)}),
\end{aligned}$$

where the parton_i-parton_j differential cross sections $d\hat{\sigma}_{ij}/d\hat{t}$ are evaluated at the lowest order in pQCD by making use of exact kinematics. The kinematical

constraints are implemented through the quantities $\Phi^{(i)}$. The expressions of $\Phi^{(i)}$ and of the invariants $\hat{s}_i, \hat{t}_i, \hat{u}_i$ are derived in great detail in the appendix.

The infrared singularity is regularized by introducing in the propagators the mass parameter p_0 , which is a free parameter in the model. Higher order effects in the elementary interaction are accounted by multiplying the lowest order expressions in α_s by the factor k_{fact} .

When evaluating the π^0 spectrum, we let partons fragment independently, neglecting the transverse momentum component generated by the fragmentation process. The relations between hadronic and partonic variables are hence the following [17]:

$$m_h \cosh y_h = z p_t \cosh y \quad m_h \sinh y_h = q_t \sinh y$$

where $z = \frac{E_h}{E}$, with E the energy of the parton, y its rapidity, E_h the energy of the hadron h , m its mass, y_h its rapidity, q_t its transverse momentum and m_h its transverse mass. The inclusive π^0 spectrum is hence given by:

$$\frac{d\sigma^{frag}}{d^2 q_t dy_h d^2 b} = \sum_i \frac{d\sigma_i^{frag}}{d^2 q_t dy_h d^2 b}$$

with

$$\frac{d\sigma_i^{frag}}{d^2 q_t dy_h d^2 b} = J(m_h, y_h) \int \frac{dz}{z^2} D_{i \rightarrow h}(z, Q_F^2) \left. \frac{d\sigma_i}{d^2 p_t dy d^2 b} \right|_{p_t, y},$$

where

$$p_t = \frac{q_t}{z} J(m_h, y_h) \quad y = \arcsin \left(\frac{m_h \sinh y}{q_t} \right)$$

$$J(m_h, y_h) = \left(1 - \frac{m_h^2}{m_h^2 \cosh^2 y_h} \right)^{-\frac{1}{2}}$$

and $D_{i \rightarrow h}(z, Q_F^2)$ the fragmentation functions, depending on the fragmentation scale Q_F . The integration region for the hadron energy fraction z is set by the request $p_t \geq p_0$, with p_0 the infrared regulator:

$$\frac{2 m_h \cosh y_h}{\sqrt{s}} \leq z \leq \min \left[1, \frac{q_t}{p_0} J(m_h, y_h) \right].$$

2.1 Numerical Results

In our calculations we use the isospin averaged nuclear parton distributions, $f_{\frac{A}{A}} = Z f_{\frac{1}{p}} + (A - Z) f_{\frac{1}{n}}$, where for the proton and the neutron distributions, $f_{\frac{1}{p}}$ and $f_{\frac{1}{n}}$, we take the CTEQ5 parametrization at the leading order [18], while for the nuclear thickness function $T_A(b)$, which is normalized to one, we use

the Wood-Saxon parametrization. At $\sqrt{s} = 200$ AGeV the differences between partons are explicitly taken into account, both in the distributions and in the evaluation of the partonic cross sections. At $\sqrt{s} = 6$ ATeV, given the small values of x in the kinematical range considered, we use effective parton distribution functions with the gluon-gluon cross-section as a dynamical input.

When considering the LHC regime, we set the factorization and renormalization scale Q_{fct} , Q_{rn} equal to the regularized transverse mass $m_t = \sqrt{p_0^2 + p_t^2}$. The transverse spectrum of jets, in proton-lead collisions at $\sqrt{s} = 6$ ATeV and within the interval $\eta \in [3, 4]$ (corresponding to the acceptance of the LHCb detector) is evaluated by the expression:

$$\frac{dW_{pA}}{d^2p_t} = \frac{1}{y_{max} - y_{min}} \int_{y \in [y_{min}, y_{max}]} dx d^2b \frac{d\sigma}{d^2p_t dy d^2b}; \quad (5)$$

where the integrand is given by Eq.(3). We consider two different choices of the infrared regulator $p_0 = 1, 2$ GeV and we use $k_{factor} = 2$.

Our results are plotted in Fig.1, where we compare the spectrum (5) obtained by the exact implementation of energy conservation in the multiple interactions (solid line), with the approximate kinematics results given by the first three terms of the expansion of Eq.(1). As an effect of the exact implementation of kinematics the spectrum of the outgoing particle is shifted towards lower transverse momenta, resulting in an appreciable energy loss effect: at $p_t \sim 15$ GeV the energy-loss correction to the spectrum is of the order of 40-45%, at higher transverse momenta, $p_t \sim 30$ GeV, it's still about 33-35% . The triple scattering approximation, used to evaluate the spectrum, breaks down at $p_t \leq 6$ GeV, when using $p_0 \sim 1$ GeV (left panel of Fig.1), while increasing the regulator up to the value $p_0 = 2$ GeV, the region of numerical instability is shifted to the region with $p_t \leq 0.3$ GeV (right panel of Fig.1).

The softening of the spectrum has important effects on the Cronin ratio, defined as:

$$R(p_t) = \frac{dW_{pA}/d^2p_t}{dW_{pA}^{(1)}/d^2p_t}.$$

where $dW_{pA}^{(1)}/d^2p_t$ is the cross section in impulse approximation. The Cronin ratio, corresponding to the spectra in fig.1, is shown in fig.2, where the dashed and continuous lines correspond to approximate and exact kinematics respectively. The two panels refer to the two values considered for p_0 , 1 and 2 GeV respectively. While the dependence of R on p_0 is very strong, one may notice that the values of the two parameters characterizing the ratio, namely the transverse momenta p_X and p_M , defined by $R(p_X) = 0$ and $R(p_M) = R_M$, with R_M the maximum of R , depend rather smoothly on p_0 and may hence be regarded as well defined predictions of the model. The overall effect of the implementation of energy conservation on R is hence to decrease the size of the Cronin effect and to shift the curve towards smaller transverse momenta.

At lower energy, $\sqrt{s} = 200$ AGeV, we follow [10] in the evaluation of the cross section of $d + Au \rightarrow \pi^0 X$, using $Q_{fct} = Q_{rn} = \frac{m_t}{2}$, and the values $p_0 = 1.0$ GeV and $k_{fact} = 1.04$. These choices, besides minimizes the effects of higher order corrections in α_S , allow one reproducing the inclusive cross section of π^0 production in pp collisions at the same c.m. energy, without any need of smearing the cross section with an intrinsic parton transverse momentum. The resulting Cronin ratio in $d + Au$ collisions is hence a parameter free prediction of the our model.

By using the leading order $K\text{-}K\text{-}P$ fragmentation functions [19] at the fragmentation scale $Q_F = \frac{m_t}{2}$, we evaluate:

$$R_{dAu \rightarrow \pi^0 X} = \frac{d\sigma_{dAu \rightarrow \pi^0 X}^{frag}}{d^2 q_t dy d^2 b} \Big/ \frac{d\sigma_{dAu \rightarrow \pi^0 X}^{frag(1)}}{d^2 q_t dy d^2 b}$$

at $y = 0$ and $b = b_{dAu} = 5.7\text{ fm}$, which is the estimated average impact parameter of the experiment [20]. In fig.3 we compare our result (continuous line) with the experimental data of the PHENIX collaboration [11] and with the result obtained by using the approximate kinematics of Eq.(1), dashed line. Given the small rapidity values of the observed π^0 , in this case the corrections induced by exact kinematics are particularly important in the region of smaller transverse momenta.

Our result shows an improved agreement of the model with the experimental data.

2.2 Conclusions

The interaction probabilities, of processes with momentum transfer well above the lower limit for a perturbative approach, become very large in proton-nucleus collisions at very high energy. In this regime unitarity needs to be implemented already at the level of perturbative interactions and the Glauber-Eikonal model of multiple parton collisions allows implementing unitarity in the simplest and most natural way. A standard approximation is to conserve the longitudinal momentum components of the projectile during the interaction. The approximation becomes however questionable when dealing with parton interactions, since parton distributions are singular at small x and a small change of the parton momentum leads to sizable modifications of the initial parton flux.

In the present note we have studied this particular aspect of the problem, working out the leading terms in the expansion in multiple parton collisions and taking into account all kinematical constraints exactly. Our result is that the spectrum of the produced large p_t partons is appreciably softened after implementing exact kinematics.

The Cronin effect has been recently measured in the large p_t spectrum of π^0 production in proton-lead collisions, at $y = 0$ and $\sqrt{s} = 200$ AGeV. We have worked out the π^0 spectrum in the same kinematical conditions and found a rather good agreement of our model with experimental data. In this particular case the corrections to the Glauber Eikonal model, induced by implementing

kinematics exactly, are increasingly important in the region of smaller p_t , where, given the rapidity value of the observed π^0 , longitudinal and transverse momentum components are of comparable magnitude.

Acknowledgments

We are grateful to M. Tosolini for his valuable computational support. One of us, D.T., thanks the Department of Energy's Institute for Nuclear Theory at the University of Washington for hospitality and the Department of Energy for partial support during the completion of this work. This work was partially supported by the Italian Ministry of University and of Scientific and Technological Researches (MIUR) by the Grant COFIN2003.

Appendix: Scattering Kinematics

The four-body parton interaction (one projectile parton against three target partons) is represented in the model by the convolution of three on-shell elastic parton-parton scatterings. We call h the four-momentum of the initial state projectile parton, and p', p'', p''' , the four-momenta of the three nuclear target partons. All partons are massless and on shell and have zero transverse momentum components. By introducing the momentum fractions x, x', x'' , the light-cone components of the four momenta in the initial state are:

$$h = (\sqrt{s}x, 0; \bar{0}) \quad p' = (0, \sqrt{s}x'; \bar{0}) \quad p'' = (0, \sqrt{s}x''; \bar{0}) \quad p''' = (0, \sqrt{s}x'''; \bar{0})$$

The transverse components of the exchanged four-momenta are \bar{q}_1, \bar{q}_2 and \bar{q}_3 , while I, J, K are the projectile's four-momenta after the first, second and third interaction and P, Q and R the four-momenta of the recoiling target partons. For the transverse components one has:

$$I_\perp = \bar{q}_1 \quad J_\perp = \bar{q}_1 + \bar{q}_2 \quad K_\perp = \bar{q}_1 + \bar{q}_2 + \bar{q}_3 \quad P_\perp = -\bar{q}_1 \quad Q_\perp = -\bar{q}_2 \quad R_\perp = -\bar{q}_3$$

While the energy conservation and mass-shell conditions, for each two-body scattering process, are expressed by the following equations:

$$\begin{cases} I^+ I^- = \bar{q}_1^2 \\ P^+ P^- = \bar{q}_1^2 \\ \sqrt{s}x = I^+ + P^+ \\ \sqrt{s}x' = I^- + P^- \end{cases} \quad (6)$$

$$\begin{cases} J^+ J^- = (\bar{q}_1 + \bar{q}_2)^2 \\ Q^+ Q^- = \bar{q}_2^2 \\ I^+ = J^+ + Q^+ \\ I^- + \sqrt{s}x'' = J^- + Q^- \end{cases} \quad (7)$$

$$\begin{cases} K^+ K^- = (\bar{q}_1 + \bar{q}_2 + \bar{q}_3)^2 \\ R^+ R^- = \bar{q}_3^2 \\ J^+ = K^+ + R^+ \\ J^- + \sqrt{s}x''' = K^- + R^- \end{cases} \quad (8)$$

The three systems of equations allow to determine

$$x, I^+, I^-, J^+, J^-, K^-, P^+, P^-, Q^+, Q^-, R^+, R^-$$

as a function of $\bar{q}_1, \bar{q}_2, \bar{q}_3, K^+, x', x''$ and x''' .

From the system (8) and the mass shell condition $J^+ J^- = (\bar{q}_1 + \bar{q}_2)^2$, one obtains:

$$\begin{aligned} (\sqrt{s}x''' K^+ - (\bar{q}_1 + \bar{q}_2 + \bar{q}_3)^2) (J^+)^2 - (\bar{q}_1 + \bar{q}_2)^2 (K^+)^2 \\ - (\sqrt{s}x''' K^+ - 2 (\bar{q}_1 + \bar{q}_2) \cdot (\bar{q}_1 + \bar{q}_2 + \bar{q}_3)) J^+ K^+ = 0 \end{aligned}$$

which has real solutions when $\Lambda^{(3)} \geq 0$, where

$$\begin{aligned} \Lambda^{(3)} = & (\sqrt{s}x''' K^+)^2 - 4 (\bar{q}_1 + \bar{q}_2) \cdot \bar{q}_3 \sqrt{s}x''' K^+ \\ & + 4 \left(((\bar{q}_1 + \bar{q}_2) \cdot \bar{q}_3)^2 - (\bar{q}_1 + \bar{q}_2)^2 \bar{q}_3^2 \right) \end{aligned}$$

The condition $\Lambda^{(3)} \geq 0$ can be satisfied only if $\Phi^{(3)} \geq 0$, where:

$$\Phi^{(3)} = 1 - 2 \frac{((\bar{q}_1 + \bar{q}_2) \cdot \bar{q}_3 + |\bar{q}_1 + \bar{q}_2| |\bar{q}_3|)}{\sqrt{s}x''' K^+} \quad (9)$$

which gives the kinematical limits for x''' and for K^+

$$x'''_{min} \equiv \frac{2((\bar{q}_1 + \bar{q}_2) \cdot \bar{q}_3 + |\bar{q}_1 + \bar{q}_2| |\bar{q}_3|)}{\sqrt{s}x''' K^+} \equiv \frac{K^+_{min}}{K^+} \leq 1 \quad (10)$$

One hence obtains J and R :

$$\begin{aligned} J^+ &= \frac{K^+}{2} \cdot \frac{\sqrt{s} K^+ x''' - 2 ((\bar{q}_1 + \bar{q}_2) \cdot (\bar{q}_1 + \bar{q}_2 + \bar{q}_3)) + \sqrt{\Lambda^{(3)}}}{\sqrt{s} K^+ x''' - (\bar{q}_1 + \bar{q}_2 + \bar{q}_3)^2} \\ J^- &= \frac{\sqrt{\Lambda^{(3)}} + 2 ((\bar{q}_1 + \bar{q}_2) \cdot (\bar{q}_1 + \bar{q}_2 + \bar{q}_3)) - \sqrt{s} K^+ x'''}{2 K^+} \\ R^+ &= \frac{K^+}{2} \cdot \frac{\sqrt{\Lambda^{(3)}} + 2 (\bar{q}_3 \cdot (\bar{q}_1 + \bar{q}_2 + \bar{q}_3)) - \sqrt{s} K^+ x'''}{\sqrt{s} K^+ x''' - (\bar{q}_1 + \bar{q}_2 + \bar{q}_3)^2} \\ R^- &= \frac{\sqrt{\Lambda^{(3)}} + \sqrt{s} K^+ x''' - 2 (\bar{q}_3 \cdot (\bar{q}_1 + \bar{q}_2 + \bar{q}_3))}{2 K^+}, \end{aligned}$$

while the Mandelstam invariants $\hat{s}_3 = (J + p'')^2$, $\hat{t}_3 = (K - J)^2$, $\hat{u}_3 = (R - J)^2$ are expressed by:

$$\begin{aligned}\hat{s}_3 &= \sqrt{s} x'' J^+ \\ \hat{t}_3 &= - \frac{((\bar{q}_1 + \bar{q}_2 + \bar{q}_3) J^+ - K^+ (\bar{q}_1 + \bar{q}_2))^2}{K^+ J^+} \\ \hat{u}_3 &= - \frac{(J^+ \bar{q}_3 + R^+ (\bar{q}_1 + \bar{q}_2))^2}{J^+ R^+}\end{aligned}\quad (11)$$

After solving (7) with respect to I and Q as a function of \bar{q}_1 , \bar{q}_2 , \bar{q}_3 , J^+ and x'' and using the mass shell condition $I^+ I^- = \bar{q}_1^2$ one obtains:

$$\begin{aligned}\left(\sqrt{s} x'' J^+ - (\bar{q}_1 + \bar{q}_2)^2 \right) (I^+)^2 - (\bar{q}_1)^2 (J^+)^2 \\ - \left(\sqrt{s} x'' J^+ - 2 \bar{q}_1 \cdot (\bar{q}_1 + \bar{q}_2) \right) I^+ J^+ = 0\end{aligned}$$

which has real solutions when $\Lambda^{(2)} \geq 0$, where

$$\Lambda^{(2)} = (\sqrt{s} x'' J^+)^2 - 4 \bar{q}_1 \cdot \bar{q}_2 \sqrt{s} x'' J^+ + 4 \left((\bar{q}_1 \cdot \bar{q}_2)^2 - \bar{q}_1^2 \bar{q}_2^2 \right).$$

The condition $\Lambda^{(2)} \geq 0$ is satisfied only if $\Phi^{(2)} \geq 0$, where

$$\Phi^{(2)} = 1 - 2 \frac{(\bar{q}_1 \cdot \bar{q}_2 + |\bar{q}_1| |\bar{q}_2|)}{\sqrt{s} x'' J^+} \quad (12)$$

which gives the kinematical limits for x'' and for K^+

$$x''_{min} \equiv \frac{2 (\bar{q}_1 \cdot \bar{q}_2 + |\bar{q}_1| |\bar{q}_2|)}{\sqrt{s} x'' J^+} \equiv \frac{J^+_{min}}{J^+} \leq 1 \quad (13)$$

One hence obtains I and Q :

$$\begin{aligned}I^+ &= \frac{J^+}{2} \cdot \frac{\sqrt{s} J^+ x'' - 2 (\bar{q}_1 \cdot (\bar{q}_1 + \bar{q}_2)) + \sqrt{\Lambda^{(2)}}}{\sqrt{s} J^+ x'' - (\bar{q}_1 + \bar{q}_2)^2} \\ I^- &= \frac{\sqrt{\Lambda^{(2)}} + 2 (\bar{q}_1 \cdot (\bar{q}_1 + \bar{q}_2)) - \sqrt{s} J^+ x''}{2 J^+} \\ Q^+ &= \frac{J^+}{2} \cdot \frac{\sqrt{\Lambda^{(2)}} + 2 (\bar{q}_2 \cdot (\bar{q}_1 + \bar{q}_2)) - \sqrt{s} J^+ x''}{\sqrt{s} J^+ x'' - (\bar{q}_1 + \bar{q}_2)^2} \\ Q^- &= \frac{\sqrt{\Lambda^{(2)}} + \sqrt{s} J^+ x'' - 2 (\bar{q}_2 \cdot (\bar{q}_1 + \bar{q}_2))}{2 J^+},\end{aligned}$$

while the Mandelstam invariants $\hat{s}_2 = (I^+ + p'')^2$, $\hat{t}_2 = (J - I)^2$, $\hat{u}_2 = (I - Q)^2$ are given by:

$$\begin{aligned}
\hat{s}_2 &= \sqrt{s} x'' I^+ \\
\hat{t}_2 &= -\frac{((\bar{q}_1 + \bar{q}_2) I^+ - J^+ \bar{q}_1)^2}{I^+ J^+} \\
\hat{u}_2 &= \frac{(I^+ \bar{q}_2 + Q^+ \bar{q}_1)^2}{I^+ Q^+}
\end{aligned} \tag{14}$$

By solving (6) with respect to x and P as a function of x' , I and \bar{q}_1 one obtains:

$$\begin{aligned}
x &= \frac{x' I^+}{\sqrt{s} x' - I^-} \\
P^+ &= \frac{\bar{q}_1^2}{\sqrt{s} x' - I^-} \\
P^- &= \sqrt{s} x' - I^-
\end{aligned} \tag{15}$$

The lower limit of x' is derived when requiring x to be smaller than 1:

$$x' \geq x'_{min} \equiv \frac{I^-}{\sqrt{s} - I^+} \tag{16}$$

so we introduce

$$\Phi^{(1)} = 1 - \frac{I^-}{x' (\sqrt{s} - I^+)} \tag{17}$$

while the expression of the Mandelstam invariants $\hat{s}_1 = (h + p)^2$, $\hat{t}_1 = (I - h)^2$ and $\hat{u}_1 = (P - h)^2$ is:

$$\begin{aligned}
\hat{s}_1 &= s x x' \\
\hat{t}_1 &= -\sqrt{s} x' I^+ \\
\hat{u}_1 &= -\sqrt{s} x P^-
\end{aligned} \tag{18}$$

References

- [1] A. Accardi *et al.*, arXiv:hep-ph/0308248.
- [2] D. Antreasyan, J. W. Cronin, H. J. Frisch, M. J. Shochet, L. Kluberg, P. A. Piroue and R. L. Sumner, Phys. Rev. D **19**, 764 (1979).
- [3] P. B. Straub *et al.*, 38.8-Gev," Phys. Rev. Lett. **68**, 452 (1992).

- [4] M. Gyulassy and P. Levai, Phys. Lett. B **442**, 1 (1998) [arXiv:hep-ph/9807247].
- [5] X. N. Wang, Phys. Rev. C **61**, 064910 (2000) [arXiv:nucl-th/9812021].
- [6] E. Wang and X. N. Wang, Phys. Rev. C **64**, 034901 (2001) [arXiv:nucl-th/0104031].
- [7] Y. Zhang, G. Fai, G. Papp, G. G. Barnafoldi and P. Levai, Phys. Rev. C **65**, 034903 (2002) [arXiv:hep-ph/0109233].
- [8] B. Z. Kopeliovich, J. Nemchik, A. Schafer and A. V. Tarasov, Phys. Rev. Lett. **88**, 232303 (2002) [arXiv:hep-ph/0201010].
- [9] M. A. Braun, E. G. Ferreiro, C. Pajares and D. Treleani, Nucl. Phys. A **723**, 249 (2003) [arXiv:hep-ph/0207303].
- [10] A. Accardi and M. Gyulassy, arXiv:nucl-th/0308029.
- [11] S. S. Adler *et al.* [PHENIX Collaboration], collisions,” Phys. Rev. Lett. **91**, 072303 (2003) [arXiv:nucl-ex/0306021].
- [12] A. Accardi and M. Gyulassy, Proc. 19th Winter Workshop on Nuclear Dynamics (2003).
- [13] A. Accardi and D. Treleani, Phys. Rev. D **64**, 116004 (2001) [arXiv:hep-ph/0106306].
- [14] V. M. Braun and Y. M. Shabelski, Int. J. Mod. Phys. A **3**, 2417 (1988).
- [15] A. Accardi and D. Treleani, Phys. Rev. D **63**, 116002 (2001) [arXiv:hep-ph/0009234].
- [16] V. Abramovskii, V.N. Gribov and O.V. Kancheli, *Yad. Fiz.* **18**, 595 (1973) [*Sov. J. Nucl. Phys.* **18**, 308 (1974)].
- [17] K. J. Eskola and H. Honkanen, arXiv:hep-ph/0205048.
- [18] H. Lai *et al.* [CTEQ Collaboration], Eur. Phys. J. C **12** (2000) 375
- [19] B. A. Kniehl, G. Kramer and B. Potter, Nucl. Phys. B **582** (2000) 514
- [20] K. J. Eskola, K. Kajantie, and J. Lindsford, Nucl. Phys. B **323** (1989) 37.

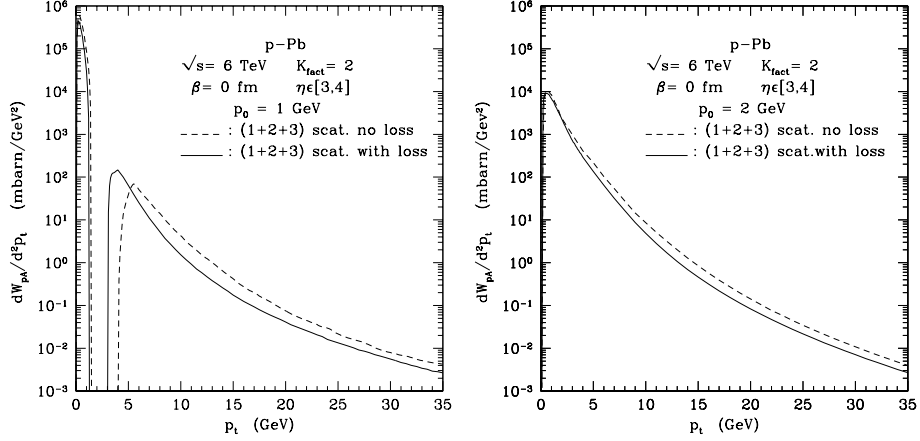


Figure 1: Transverse momentum spectrum of partons produced in $p + Pb$ collisions at $\sqrt{s} = 6$ ATeV and $\eta \in [3, 4]$, using $p_0 = 1, 2$ GeV, and $k_{\text{factor}} = 2$. The solid lines are the result of implementing exact kinematics in the calculation, the dashed lines refer to the case of approximate kinematics

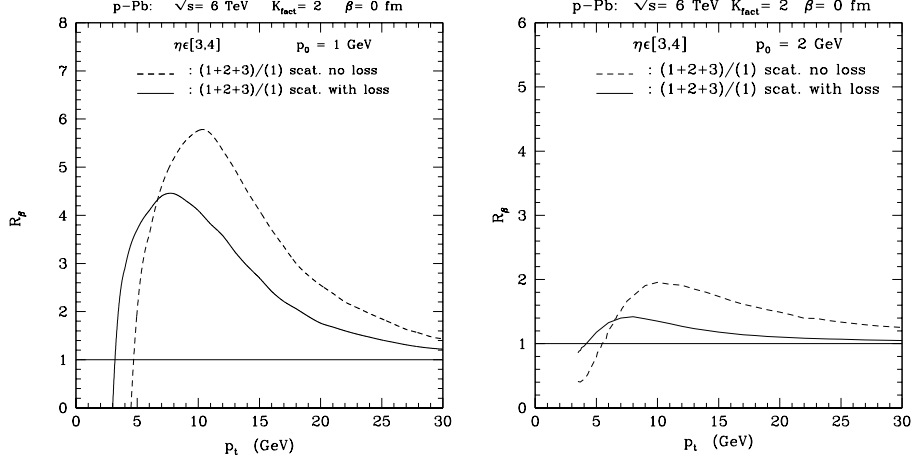


Figure 2: Cronin Ratio in the case of exact kinematics (solid line) and in the case of approximate kinematics (dashed line)

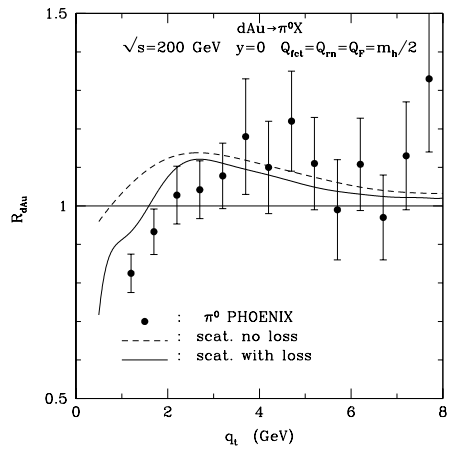


Figure 3: Cronin ratio in $d + Au \rightarrow \pi^0 X$ collisions at $\sqrt{s} = 200$ GeV. The solid line refers to the case of exact kinematics and the dashed line to the case of approximate kinematics. The data are from ref.[11]